ELSEVIER

Polymer 43 (2002) 5527–5534

polymer

www.elsevier.com/locate/polymer

Structure and property studies of bioabsorbable poly(glycolide-*co*-lactide) fiber during processing and in vitro degradation

Bruce X. Fu[a], Benjamin S. Hsiao[a], Gavin Chen[b,*], Jack Zhou[b,*], Ilya Koyfman[b], Dennis D. Jamiolkowski[b], Edward Dormier[b]

[a]*Department of Chemistry, State University of New York at Stony Brook, Stony Brook, NY 11794-3400, USA*
[b]*Ethicon Worldwide, A Johnson & Johnson Company, P.O. Box 151, Somerville, NJ 08876-0151, USA*

Received 28 February 2002; received in revised form 6 June 2002; accepted 10 June 2002

Abstract

Structure and properties of a bioabsorbable poly(glycolide-*co*-lactide) (PGA-*co*-PLA) fiber during several processing stages and the final in vitro degradation stage were investigated by means of wide-angle X-ray diffraction, dynamic mechanical analysis and mechanical property tests. In the orientation stage, an increase in the temperature of the first encountered orientation roll resulted in a lower level of crystallinity and larger crystallites. The temperature of the second encountered pre-annealing roll (PR) imposed a smaller effect on the structure. In the hot-stretching stage after fibers were braided, the maximum crystallinity was achieved at around 126 °C. Higher hot-stretching temperatures increased the crystal size, glass transition temperature (T_g) and tensile strength, but decreased the elongation at break and the heat shrinkage near T_g. In the post-annealing stage, it was found that crystallinity, T_g and tensile strength all increased significantly while the heat shrinkage near T_g sharply decreased after annealing. This suggests that the internal stress accumulated in the orientation and hot-stretching stages can be effectively reduced by post-annealing. During in vitro degradation, crystallinity was found to increase with time while the heat shrinkage near T_g and in the supercooling region ($T_g < T < T_m$) was greatly reduced. These results support the process of cleavage-induced crystallization.

Keywords: Poly (glycolide-*co*-lactide); Bioabsorbable; Fiber

1. Introduction

Bioabsorbable polymers are an important class of synthetic biomaterials that are widely used in temporary therapeutic applications such as wound closure, tissue regeneration and drug delivery. Most of these polymers have degradable backbones that are composed of esters, anhydrides, carbonates, urethanes and so forth. Among the bioabsorbable polymers developed thus far, polyglycolide (PGA), poly(L-lactide) (PLA) and their copolymers (PGA-*co*-PLA) attract the most attention in commercial applications. For many surgical repair applications, they possess suitable bioabsorbable properties as well as suitable mechanical properties. A commercial product having a proven record in clinical applications is VICRYL™ (Ethicon trademark) Suture, which is based on one of the (PGA-*co*-PLA) copolymers.

In order to produce absorbable sutures of high quality, two important properties have to be assured. One is the initial mechanical performance, especially the tensile strength of the suture that determines the capability of holding the wound tissues together. Another important property is the biological performance, which is related to the performance of the article once implanted. One aspect of this biological performance for mechanical devices is the rate at which mechanical properties are reduced. For example, in the case of sutures, the breaking strength retention profile of the fiber is crucial. Biological performance is also related to the absorption and tissue reaction profiles that are exhibited by the implanted material; these can be followed histologically. Seemingly identical materials can behave very differently with regards to their biological and mechanical performances if they display different morphologies. Many studies have been carried out to investigate the structure and property relationship in PGA and PLA fibers [1–7]. It was found that higher crystallinity and molecular orientation usually resulted in higher tensile strength and lower degradation rate.

A widely used model to describe the structure of PGA-*co*-PLA fiber is the two-phase model; it assumes the fiber

* Corresponding authors.

0032-3861/01/$ - see front matter
PII: S0032-3861(02)00389-0

structure is made of alternate crystalline and amorphous phases. A single chain may enter multiple crystal and amorphous domains. The crystalline phase is primarily composed of chain segments in ordered conformation, whereas the amorphous phase contains chain ends, entangled chains and segments in some disordered conformation. During degradation, it has been reported that the hydrolysis process consists of two major mechanisms [8–15]. In the first mechanism, water molecules diffuse into the amorphous region, resulting in scission of some disordered chains. The densely ordered crystalline phase, which is more difficult for water to penetrate, stays largely unaffected. As water molecules react with the amorphous chain segments (e.g. begin to hydrolyze ester groups, if the polymer is an absorbable polyester), these cleaved disordered chains can disentangle as their mobility is significantly improved. The additional degree of freedom facilitates the formation of new crystalline regions and increases the overall crystallinity. This phenomenon is termed 'cleavage-induced crystallization' [14]. As a result, the crystallinity will reach a maximum, which marks the initiation of the second mechanism. Water molecules can slowly attack the crystalline phase resulting in chain segments small enough to be water soluble and susceptible to metabolism. It is conceivable that the weight loss of amorphous phase during degradation can also contribute to the increase in crystallinity observed in the early stages of degradation [14]. However, we believe that this contribution is much smaller than that from the cleavage-induced crystallization as the true loss of the chain fractions may not be too big in these stages.

It is well known that the degree of crystallinity and mechanical properties of polymeric fibers can be greatly influenced by processing conditions [1,2,6]. In typical fiber processing, two process techniques are routinely used to manipulate the fiber properties. One technique involves the orientation process and the other technique involves the annealing process (or heat-setting process). The orientation process imposes a mechanical stretching of the polymer chains and crystallites, thus results in an increase of crystalline orientation and crystallinity. These changes in structure usually yield an increase in tensile strength but a decrease in elongation. The orientation process can be greatly influenced by two factors: the draw ratio and the draw temperature. A higher draw ratio usually results in higher tensile strength but a lower elongation at break. During the annealing process (heat-setting), the polymer chains gain mobility due to the elevated temperature. As a result, the molecular segments in lower order tend to crystallize. This process often yields an increase in crystallinity, but may lose a certain degree of crystalline orientation and cause the fiber to shrink. In this study, we have examined the structure and property changes during many different fiber process stages. We also investigated the degradation process of the oriented and braided fibers in an accelerated in vitro test.

2. Experimental

2.1. Materials and sample preparation

Samples used in this study were random copolymers based on approximately 90 mol% glycolide and 10 mol% L-lactide (90/10 PGA-*co*-PLA). This resin had a M_w of 60,000, a M_n of 22,000 and a polydispersity of 2.8. The polymer was stored under vacuum before extrusion. The polymer was extruded and processed using the procedures schematically shown in Fig. 1. The identification of the samples is as follows: Drawn fibers (Table 1) were labeled V1A to V1J, respectively. Samples after the braiding and scouring stages were labeled by adding two letters 'BS' after the corresponding name of the drawn fibers. For instance, sample V1A became V1A_BS for braided fibers. The hot-stretched samples were indicated by adding a letter 'H'. For instance, sample V1A_BS became V1A_BSH. The annealed samples were designated by adding a letter 'A' after the corresponding name of the hot-stretched samples.

The annealed samples were placed in a buffer solution (pH 7.79) at 40.9 °C for in vitro degradation study. A small amount of sample was taken out and dried after a certain period of time for structure and property tests. The in vitro degraded samples were named by adding the number of days of exposure. For instance, after 8 days of degradation, sample V1A_BSHA became V1A_BSHA_8D.

2.2. Wide-angle X-ray diffraction

The X-ray measurements were carried out on a Siemens

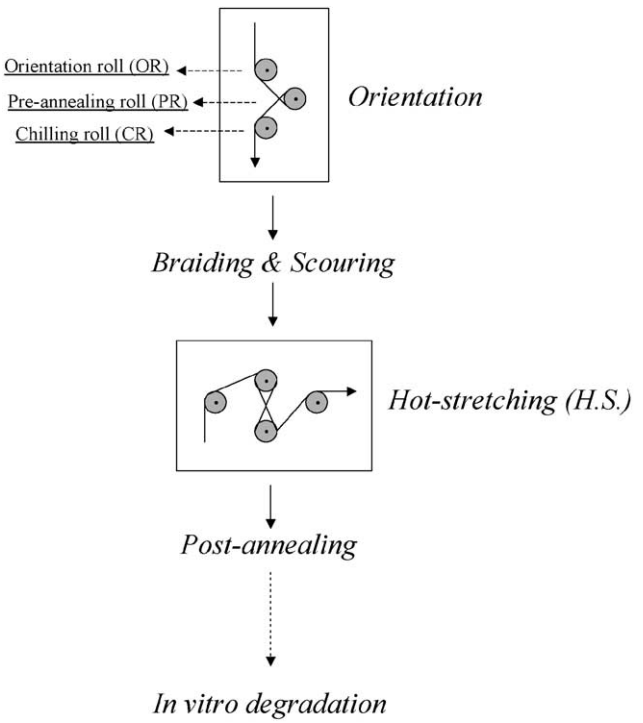

Fig. 1. Schematic drawing of the various fiber processing stages.

Table 1
Structure and property parameters of the PGA-*co*-PLA fibers produced at different PR and OR temperatures in the orientation stage

Sample name	Crystallinity (%)	Crystal size (Å)	Tenacity (gpd)	Elongation at break (%)	Processing temperatures
V1A	23	46	6.9 ± 0.3	24 ± 1	OR = 84 °C, PR = 121 °C
V1B	23	46	5.8 ± 0.3	28 ± 2	OR = 84 °C, PR = 111 °C
V1C	23	46	6.1 ± 0.2	27 ± 2	OR = 84 °C, PR = 101 °C
V1D	22	44	6.3 ± 0.2	28 ± 2	OR = 84 °C, PR = 91 °C
V1E	18	45	6.2 ± 0.2	30 ± 2	OR = 84 °C, PR = 81 °C
V1F	8	31	4.7 ± 0.2	30 ± 2	OR = 84 °C, PR = 61 °C
V1G	18	44	5.9 ± 0.4	29 ± 2	OR = 90 °C, PR = 81 °C
V1H	22	42	6.8 ± 0.3	27 ± 1	OR = 80 °C, PR = 81 °C
V1I	23	39	6.4 ± 0.3	21 ± 1	OR = 70 °C, PR = 81 °C
V1J	23	40	5.7 ± 0.3	18 ± 1	OR = 60 °C, PR = 81 °C

Hi-Star™ unit with Cu Kα radiation at a wavelength of 1.542 Å. The instrument was operated at 40 kV and 40 mA with a collimator size of 0.5 mm. The fiber sample was mounted on a goniometer, normal to the X-ray beam. The exposure time for each sample was 300 s. The calculation of the crystallinity content was performed with DIF-FRAC PLUS™ software developed by Siemens. A 2θ-intensity profile was firstly achieved by integration of azimuthal scans with the beam stop as the center. The profile was then peak-fitted to separate the amorphous peak (a Pearson VII split peak determined by a quenched extrudate sample) and three Gaussian crystalline peaks (110, 020, 002 reflection from an orthorhombic unit cell with $a = 5.22$ Å, $b = 6.19$ Å, and $c = 7.02$ Å according to Chatani et al. [16]). Dividing the area of the crystalline peaks, I_c, by the overall area I_{total} (amorphous and crystalline areas combined), we obtained the total crystallinity of the sample. The 110 reflection peak was used to determine the crystallite size. This measurement was performed using the Scherrer equation:

$$D_{hkl} = (K\lambda 57.3)/((B - b)\cos\theta) \quad (1)$$

where K is the shape factor ($= 0.9$), λ the wavelength (1.54 Å), B the experimental breadth at the maximum intensity, and b is the instrumental correction coefficient (0.6781). We note that the observed crystal reflections observed in the wide-angle X-ray diffraction (WAXD) patterns are quite sharp, which indicates that the distortion in the crystal is small and that the reflection breadth is mostly due to the finite crystal size.

2.3. Dynamic mechanical analysis

Dynamic mechanical analysis (DMA) was performed using a DMS 120 instrument (Seiko Instrument) operated in the tensile mode. The sample was mounted on the machine with a constant 20 g tension applied during the experiments. The experiment was performed at 1 Hz with a stretching ratio of 0.1%. Samples were heated from room temperature to 180 °C at 2 °C/min. The heat shrinkage was monitored by comparing the sample length changes to the original sample length (20 mm). We note that the T_g value indicated in this paper was determined by the tan δ peak, which usually is higher than the T_g value measured by differential scanning calorimetry.

2.4. Mechanical property test

Mechanical property test was performed using an Instron tensile machine (model 4201) with a crosshead speed of 12 in/min. The maximum tensile strength and elongation at break were obtained by taking average values of eight separate measurements.

3. Results and discussion

3.1. The effect of draw temperature on fibers

By varying orientation roll (OR) and pre-annealing roll (PR) temperatures, two series of drawn fibers were produced using the same draw ratio. Table 1 shows the mechanical properties of samples V1A to V1F having a fixed OR temperature at 84 °C, but varying the PR temperatures from 121 to 61 °C. The corresponding changes in crystallinity and crystalline size at different OR and PR temperatures are shown in Fig. 2. As seen in Table 1, samples V1G to V1J were produced with varying OR temperatures ranging from 90 to 60 °C, but at a fixed PR temperature of 81 °C. Under these conditions, when the OR temperature was decreased, the elongation at break decreased significantly while crystallinity increased slightly. This suggests that at low OR temperatures in the orientation stage, a large amount of small crystallites are formed by the process of nucleation-controlled kinetics. Although the crystalline size is small, the overall crystallinity is high at low OR temperatures. The OR temperature, obviously, plays a significant role in forming the initial structure and morphology of the fibers.

The effect of the PR temperature is discussed next. It is seen in Fig. 2B that the samples made at relatively low PR temperatures (61 and 81 °C) exhibit low crystallinity and smaller crystalline size. This result indicates that the polymer chains do not crystallize well at those low temperatures. The crystalline size had increased with the

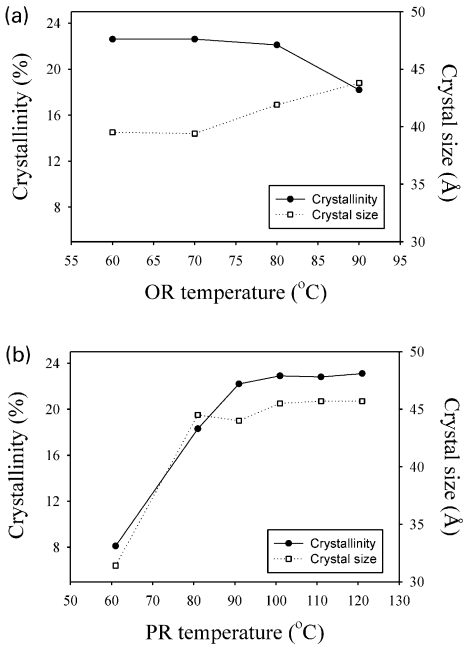

Fig. 2. Crystallinity and crystal size data of the drawn fibers in the orientation stage at different (a) PR temperatures, and (b) OR temperatures.

increase of PR temperature (Fig. 2B); this trend is similar to the one in Fig. 2A. In these samples, the crystallinity and crystalline size reach plateau values of approximately 22% and 45 Å, respectively. This suggests that after exceeding a critical value, the PR temperature has only a limited influence on structural development. The corresponding tenacity and elongation at break remain practically unchanged in samples V1B to V1E (PR temperature from 111 to 81 °C).

3.2. The effect of hot stretching temperature on fibers

In order to study the temperature effect at the hot-stretching stage, a PGA-*co*-PLA drawn fiber (V2) was firstly braided and then subjected to a hot-stretching process at different temperatures: 71, 86, 101, 126 and 131 °C. The fiber (V2) was drawn using an OR temperature of 84 °C and a PR temperature of 101 °C, resulting in a crystallinity of 24.7% and a crystal size of 42.9 Å. Table 2 shows that the crystallinity of this sample increases with an increase in hot-stretching temperature from 71 to 126 °C, and then levels off when the temperature is further increased. However, the crystalline size does not show significant changes, possibly due to rather fast stretching rate (the time is too short for crystalline thickening). The stretching temperature of the braid (the so-called 'hot stretching' temperature) also exhibits a noticeable effect on fiber properties. For example, the tensile strength at break increases with increasing hot-stretching temperature from 71 to 126 °C while elongation at break decreases. The fiber properties appear to level off when the hot-stretching temperature increases further.

DMA results show that T_g, identified as the peak position of the tan δ curve, increases with increasing hot stretching temperature (Fig. 3, upper curve). The increase in T_g can be attributed to the increase in molecular orientation in the amorphous phase by hot-stretching at high temperatures. It is also seen that the heat-shrinkage profile (Fig. 3, lower curve) exhibits noticeable changes in the glass transition region (50–120 °C) with varying hot-stretching temperatures. Samples made at lower stretching temperatures (such as 71, 86 and 101 °C) exhibit similar but larger values of heat shrinkage in, and above, the T_g region than samples produced at higher stretching temperatures (126 and 131 °C). The heat shrinkage, which is an indication of the internal stress remained in the polymer chains, is strongly associated with the relaxation of the oriented amorphous chains in the glass transition region. At high stretching temperatures, the polymer chains are in a more plastic state so that deformation (stretching) can be performed without inducing excessive internal stress in the amorphous chains leading to the smaller heat shrinkage in samples V2_BSH4 and V2_BSH5 (126 and 131 °C). Further discussion of the internal stress induced in the stretching and annealing stages will be elaborated later. We note that the draw ratio will also affect the T_g and heat shrinkage, but this effect will not be discussed in this paper. Herein, we try to only deal with the effect of temperature.

3.3. Structure and property relationships during post-orientation stages

Three samples (V1G, V1H and V1I) produced under different OR temperatures have been selected for investigating the structure and property relationship in each stage of the process after the orientation treatment (Fig. 1). Fig. 4 shows the heat shrinkage profiles of these three samples

Table 2
Structure and property parameters of the PGA-*co*-PLA braided fibers prepared in the hot-stretching stage at different temperatures

Sample name	Crystallinity (%)	Crystal size (Å)	Strength at break (lb)	Elongation at break (%)	Shrinkage at 80 °C (%)	Processing temperatures
V2_BS	25	43	15	28	14	OR = 90 °C, PR = 81 °C
V2_BSH1	27	41	16	21	16	HS = 71 °C
V2_BSH2	28	41	16	21	16	HS = 86 °C
V2_BSH3	29	42	17	19	17	HS = 101 °C
V2_BSH4	32	42	17	18	15	HS = 126 °C
V2_BSH5	32	44	17	18	13	HS = 131 °C

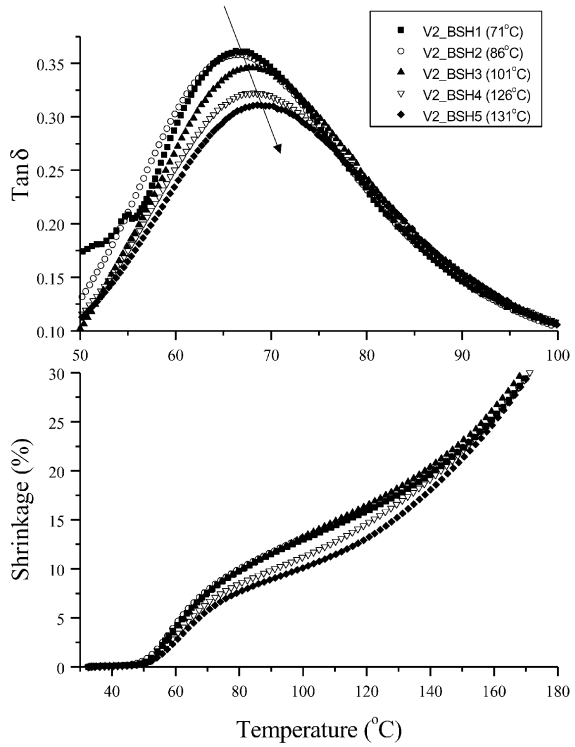

Fig. 3. DMA temperature scans of PGA-*co*-PLA sutures produced at different hot-stretching temperatures.

measured by DMA (after the braiding and scouring stages, all at room temperature). In the temperature region from 60 to 180 °C, sample V1G_BS (OR = 90 °C) is found to have much lower heat shrinkage than sample V1H_BS (OR = 80 °C) and V1I_BS (OR = 70 °C). Since the heat shrinkage behaves differently at different temperature regions, it is necessary to divide the process into three stages for discussion. The first stage is in the region $T < T_g$. As the polymer chains have very limited mobility in this region, the material usually does not show heat shrinkage. The second stage is the glass transition region ($T \sim T_g$). The polymer chains begin to gain mobility to relax from the oriented state, which results in significant heat shrinkage. This stage can be referred as the amorphous relaxation region. The last stage is the post-T_g region ($T_g < T < T_m$). In this stage, some crystalline domains (especially the regions containing chain ends, defects, and amorphous–crystalline interfaces) can gradually gain mobility, causing another significant internal stress release. This region can be referred to the crystalline relaxation region (we assume that the internal stress in the amorphous phase can be totally released by slow heating, i.e. 1–2 °C/min). In Fig. 4, we identify the amorphous relaxation region to be 50–110 °C. The crystalline relaxation phase is from 110 °C to the end of scan. As seen, these three samples have significant difference in the amorphous relaxation region. The higher the OR temperature, the lower the heat shrinkage is in the sample, assuming that the braiding and scouring stages do not play a significant role on changing the internal stress in

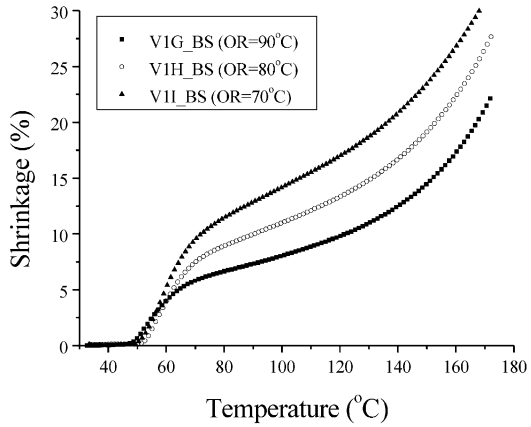

Fig. 4. The comparison of heat shrinkage profiles of PGA-*co*-PLA sutures produced at different OR temperatures.

the amorphous chains. In contrast, the crystalline relaxation region exhibits similar changes in the three samples studied (the curve shape is quite similar). This suggests that the OR temperature affects the internal stress of the amorphous chains quite significantly (the lower the OR value, the higher the internal stress), but it has a minimal effect on the crystalline phase. This is also similar to the case of the hot-stretching stage, which will be discussed next.

The structure and property relationships under different hot-stretching and annealing temperatures are summarized in Table 3. It is found that crystallinity increases after the hot-stretching and/or annealing stage. However, the crystal size shows a different trend. After the hot-stretching stage, the crystal size remains constant or even decreases slightly. This suggests that the hot-stretching process generates more crystallites with their size similar to that in the orientation stage. In contrast, the annealing stage increases the crystal size, which can be attributed to crystal perfection and/or thickening. In Table 3, the strength at break and T_g are found to increase after the hot-stretching and annealing stages. However, the T_g increase after hot-stretching is considerably less than that after annealing. Another interesting change is the half-width of the tan δ peak, which is significantly broadened after both the hot-stretching and annealing stages (the example VIH_BS sample is shown in Fig. 5, the upper plot). It is known that the tan δ peak width is related to the elasticity [17]. In the samples of narrower half-width, much of the energy is used to deform the material and is dissipated directly as heat. A completely amorphous material with Newtonian viscosity has a δ-function like tan δ peak width. A perfect elastic material such as springs will have a flat transition zone with no tan δ peak width. Therefore, the tan δ peak width increases after the hot-stretching and the annealing stages, which is consistent with induced crystallization in both stages.

In Fig. 5 (the lower plot), DMA studies show that both hot-stretching and annealing stages significantly affect the heat shrinkage of the samples. It is seen the heat shrinkage in the glass transition region is increased after hot-stretching

Table 3
Structure and property parameter changes of the PGA-*co*-PLA fibers after the combined hot-stretching and the annealing stages

Sample name	Crystallinity (%)	Crystal size (Å)	Strength at break (lb)	T_g (°C)	tan δ half-width (°C)	Shrinkage at 80 °C (%)	Processing temperatures
V1G_BS	18	44	13	60	23	6.6	OR = 90 °C, PR = 81 °C
V1G_BSH	26	41	13	61	24	8.7	HS = 71 °C
V1G_BSHA	31	45	14	75	30	3.3	Annealing temperature = 94 °C
V1H_BS	22	42	15	62	20	8.9	OR = 80 °C, PR = 81 °C
V1H_BSH	29	41	16	65	26	10.2	HS = 101 °C
V1H_BSHA	33	43	15	75	27	5.1	Annealing temperature = 94 °C
V1I_BS	23	39	14	63	20	11.5	OR = 70 °C, PR = 81 °C
V1I_BSH	28	40	16	66	25	11.1	HS = 101 °C
V1I_BSHA	36	44	16	76	29	3.7	Annealing temperature = 124 °C

(compared V1H_BS and V1H_BSH). This indicates that the stretched amorphous chains must contain some internal stress even as the deformation was carried out above T_g (the internal stress is relaxed upon heating which leads to shrinkage during the DMA measurement). In contrast, the annealing stage is found to significantly reduce the heat shrinkage of the sample above T_g. This is because the annealing stage allows some tie molecules to relax and some polymer chains to crystallize, which alleviates the internal stress and reduces the shrinkage. From the suture application standpoint, the annealing stage can significantly stabilize the mechanical properties of the fiber in the vicinity of T_g. The heat shrinkage at higher temperatures ($T_g < T < T_m$) is related to the crystallization and melting processes.

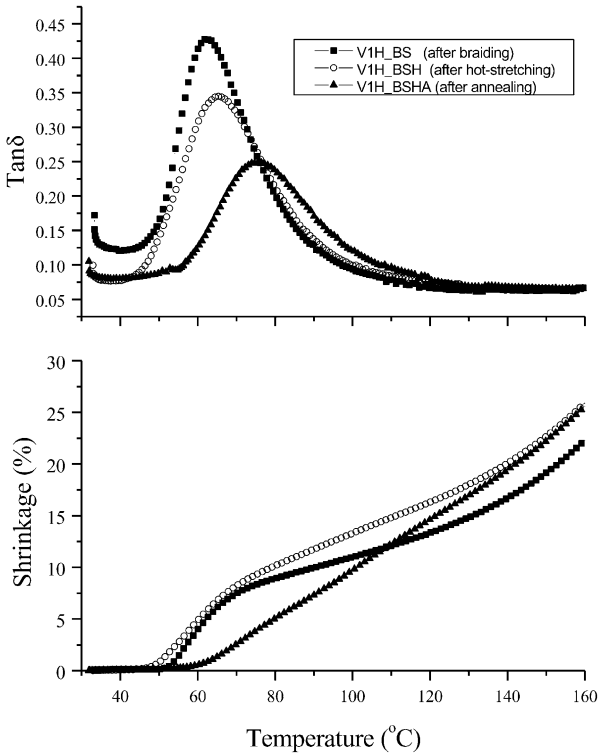

Fig. 5. An example of the tan δ and heat shrinkage changes of PGA-*co*-PLA suture as a function of temperature.

3.4. Structure and property relationships during in vitro degradation

Three samples (V1G_BSHA, V1H_BSHA and V1I_BSHA), drawn under OR temperature of 90, 80 and 70 °C, respectively, were used in an in vitro degradation study. The structure and property parameters are summarized in Table 4. It is shown that the starting samples have tensile strength of 14.4, 15.2 and 16.0 lb, respectively. Since these three samples have experienced different processing conditions, it is not surprising to find that they exhibit different crystallinities: 31.1, 33.1, and 36.1%, respectively. Fig. 6 shows the changes in crystallinity and the break strength retained (%) during in vitro degradation. It shows that the crystallinity increases with the degradation time. All of the samples exhibit a similar crystallinity value of 45 % after 20 days of degradation. Sample V1G_BSHA, which has the lowest initial crystallinity, shows the highest rate of crystallinity increase. Sample V1I_BSHA, which has the highest initial crystallinity, shows the lowest rate of crystallinity increase. These findings are consistent with the mechanism of cleavage-induced crystallization during in vitro degradation [8,14]. This process consists of two steps: (1) the cleavage of the restrained amorphous chains which results in an increase of chain mobility and loss of tensile strength, (2) the formation of crystallites from unrestrained amorphous chains during the cleavage. The chain after cleavage can crystallize at a temperature around 40 °C, much lower than the apparent T_g, because the water molecules act as plasticizers that significantly reduce the real T_g of the chains. In cleavage-induced crystallization, crystallinity will increase and reach a plateau value. Afterward, crystallinity may increase even further as hydrolysis (and loss) of amorphous regions increase the relative amount of crystallites. Even though the total amount of material is decreasing, crystallinity can increase. The data in Fig. 6 represents the early stages of cleavage-induced crystallization. The lower plot in Fig. 6 shows that the break strength retained in these samples follows an opposite trend with the degradation time. After 20 days of degradation, the break strength retained is quite negligible. No obvious

Table 4
Structure and property parameter changes of the PGA-*co*-PLA fibers during in vitro degradation

Sample name	Strength at break (lb)	Crystallinity (%)	Crystal size (Å)	T_g (°C)	tan δ half-width (°C)	Shrinkage at 120 °C (%)	M_w	M_n	M_w/M_n
V1G_BSHA_0D	14	31	45	75	30	10.8	60,000	22,000	2.8
V1G_BSHA_8D	11	34	47	73	34	4.4	34,000	14,000	2.4
V1G_BSHA_12D	9	38	45	73	37	3.0	21,000	9600	2.2
V1G_BSHA_16D	6	40	46	73	34	1.6	12,700	6700	1.9
V1G_BSHA_20D	1	46	44	78	34	1.2	6300	4200	1.5
V1H_BSHA_0D	15	33	43	75	27	14.6	60,000	22,000	2.8
V1H_BSHA_8D	12	35	44	74	31	4.9	33,000	14,000	2.4
V1H_BSHA_12D	9	38	45	71	33	2.8	20,000	9300	2.1
V1H_BSHA_16D	6	39	44	72	34	1.4	12,400	6700	1.9
V1H_BSHA_20D	1	45	44	80	31	1.3	6200	4100	1.5
V1I_BSHA_0D	16	36	44	76	29	10.1	60,000	22,000	2.8
V1I_BSHA_8D	11	37	43	75	30	4.5	36,000	15,000	2.4
V1I_BSHA_12D	10	38	45	74	35	3.1	23,000	11,000	2.1
V1I_BSHA_16D	7	41	43	73	35	2.1	16,000	8100	2.0
V1I_BSHA_20D	3	45	45	77	36	1.0	7600	4800	1.6

difference in breaking strength retention is found among the three samples, which may be due to the relatively small difference in crystallinity among these three samples.

Fig. 7 shows the DMA results for the selected samples after 8, 12, and 16 days of in vitro degradation. We note that after 20 days of degradation, the sample becomes too fragile to assure reliable DMA results (some reliable data after 20 days of degradation are included in Table 4). It is shown that T_g is slightly shifted to a lower temperature and the tan δ peak half-width slightly broadens during in vitro degradation. We note that these observations are still in the cleavage-induced crystallization time frame (the data in samples beyond 20 days of degradation is not accessible). Fig. 7 shows that the sample exhibits only little resemblance to the initial sample of lower crystallinity after 8 days of degradation. In contrast, the samples behave quite similarly after 8, 12, and 16 days of degradation. This suggests that the cleavage-induced crystallization, which initiates from the breakdown of amorphous chains, releases the internal stress immediately during in vitro degradation. The further development of cleavage-induced crystallization after 12

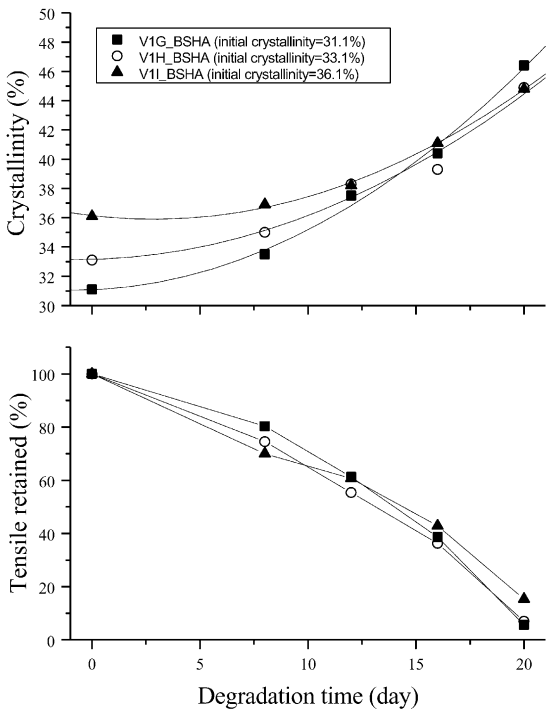

Fig. 6. The crystallinity and tensile retained percentage changes in three different PGA-*co*-PLA sutures (with different initial crystallinity) during in vitro degradation.

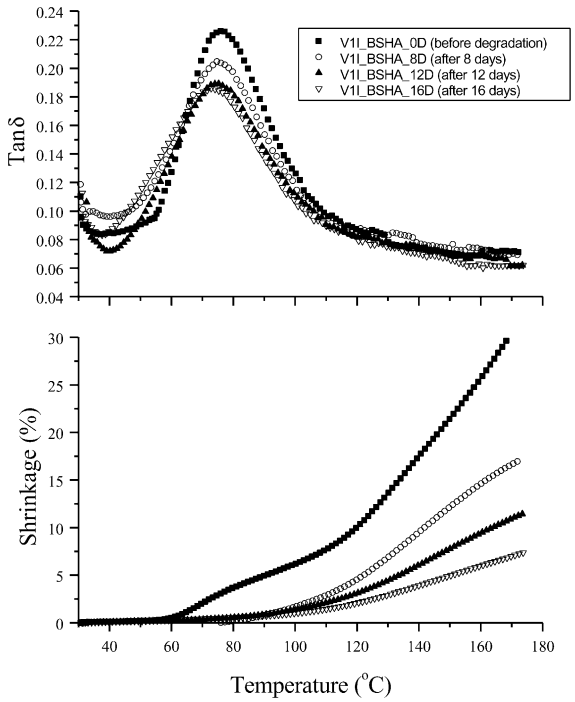

Fig. 7. An example of the tan δ and heat shrinkage changes of PGA-*co*-PLA suture samples after different in vitro degradation treatment.

and 16 days of degradation does not affect the shrinkage in the vicinity of T_g, only at much high temperatures (120–180 °C).

Other useful data in Table 4 includes the crystal size and molecular weight measured at different degradation time periods. It is shown that the crystal size is about constant during in vitro degradation, possibly due to the dominant initial crystal constituents prior to degradation. The molecular weight of the sample reduces to about one-half of its initial value after 8 days of degradation. After 16 days, the remained molecular weight in only about one-fifth of the original value. The polydispersity (M_w/M_n) is also found to decrease during in vitro degradation, which indicates that the chain length distribution becomes narrower upon degradation.

4. Conclusions

In this study, we have studied the temperature effect on structure and property of poly(glycolide-*co*-lactide) bioabsorbable fibers during several common industrial fiber processing stages and during in vitro degradation. These stages include an orientation stage, a hot-stretching stage and an annealing stage. In the orientation stage, we find that the first encountered orientation roll temperature can have a significant impact on the structure formation by the process of nucleation-controlled kinetics, while the second encountered pre-annealing roll temperature is critical to the growth of the crystallites and overall crystallinity. In the hot-stretching stage, it is found that higher hot-stretching temperature increases the tensile strength, crystallinity and crystal size. Higher hot-stretching temperature can reduce the internal stress in the restrained amorphous chains. In the annealing stage, samples can gain a significant increase in crystallinity and crystal size while heat shrinkage in the vicinity of T_g significantly decreases. The annealing process has proven to be the key step to stabilize the suture properties near T_g. All the materials examined exhibited cleavage-induced crystallization during in vitro degradation testing. It was found that the internal stress in the amorphous chains was almost completely eliminated after 8 days of degradation at the test temperature.

Acknowledgments

We would like to thank Joshua Samon, Jenny Yuan, Susan Lin, Dominick Egidio, Richard Marziaz, Donald Hill, Ray Britt, Fred Halperin, Eugene Muse, and Stephanie Duclair in Ethicon Worldwide for their assistance of the experiments. Mr John Karl of Ethicon had a critical review of the manuscript and provided several invaluable comments. This research was made possible by a Johnson & Johnson CORD Internship Award funded by Ethicon. BH and BF would also like to thank the National Science Foundation for part of the financial support (DMR-0098104).

References

[1] Penning JP, Dijkstra H, Pennings AJ. Polymer 1993;34:942.
[2] Leenslag JW, Pennings AJ. Polymer 1987;28:1695.
[3] Okuzaki H, Kubota I, Kunugi T. J Polym Sci, Polym Phys 1999;37:991.
[4] Schmack G, Tandler B, Vogel R, Beyreuther R, Jacobsen S, Fritz HG. J Appl Polym Sci 1999;73:2785.
[5] Postema AR, Pennings AJ. J Appl Polym Sci 1989;37:2351.
[6] Postema AR, Luiten AH, Pennings AJ. J Appl Polym Sci 1990;39:1265.
[7] Martin O, Averous L. Polymer 2001;42:6219.
[8] Chu CC. J Appl Polym Sci 1981;26:1727.
[9] Chu CC. J Biomed Mater Res 1981;15:19.
[10] Ginde RM, Gupta RK. J Appl Polym Sci 1987;33:2411.
[11] Fredericks RJ, Melveger AJ, Dolegiewitz LJ. J Polym Sci, Polym Phys 1984;22:57.
[12] King E, Cameron RE. J Appl Polym Sci 1997;66:1681.
[13] Zhou JJ, Samon JM, Dormier E. J Appl Med Polym 1999;3:55.
[14] Zong XH, Wang ZH, Hsiao BS, Chu B, Zhou JJ, Jamiolkowski DD, Muse E, Dormier E. Macromolecules 1999;32:8107.
[15] Wang ZG, Hsiao BS, Zong XH, Yeh F, Zhou JJ, Dormier E, Jamiolkowski DD. Polymer 2000;41:621.
[16] Chantani Y, Suehiro K, Okita Y, Tadokoro H, Chujo K. Makromol Chem 1968;113:215.
[17] Nielsen LE, Landel RF. Mechanical properties of polymers and composites, 2nd ed. New York: Marcel Dekker; 1994.